Journal of Power Sources 241 (2013) 768–775

Contents lists available at SciVerse ScienceDirect

Journal of Power Sources

journal homepage: www.elsevier.com/locate/jpowsour

LNF SOFC cathodes with active layer using Pr_6O_{11} or Pr-doped CeO_2

Hiroaki Taguchi*, Reiichi Chiba, Takeshi Komatsu, Himeko Orui, Kimitaka Watanabe, Katsuya Hayashi

NTT Energy and Environment Systems Laboratories, NTT Corporation, 3-1, Morinosato Wakamiya, Atsugi, Kanagawa 243-0198, Japan

HIGHLIGHTS

- The interface resistance, R_{inf} and overvoltage, η of the three types cathodes were investigated.
- The R_{inf} and η with cathode containing Pr_6O_{11} in the active layer exhibited the lowest at 800 °C.
- Pr_6O_{11} easily reacted with zirconia and $Pr_2Zr_2O_7$ was produced at 1000 °C or above.
- The sintering temperature of the cathodes using Pr_6O_{11} can be increased to around 1000 °C without reaction.

ARTICLE INFO

Article history:
Received 5 March 2013
Received in revised form
20 April 2013
Accepted 26 April 2013
Available online 30 May 2013

Keywords:
SOFC
Pr_6O_{11}
Cathode
Interface resistance

ABSTRACT

We fabricated electrolyte supported single cells with three types of cathodes that consisted of a $Ce_{0.1}Gd_{0.1}O_{1.95}$ (GDC) buffer layer, a $LaNi_{0.6}Fe_{0.4}O_3$ (LNF) cathode and an active layer. The only difference between the three cathodes was that each had a different active layer, namely a GDC–LNF composite active layer (our conventional cathode), a $Pr_xCe_{1-x}O_{2-\delta}$ ($x = 0.1, 0.3, 1.0$)–LNF composite active layer and a Pr_6O_{11} ($Pr_xCe_{1-x}O_{2-\delta}$ ($x = 1.0$)) active layer. The interface resistance, R_{inf}, and overvoltage, η_c, of the cathodes were investigated. At 800 °C, the R_{inf} of the cathode with the Pr_6O_{11} active layer was reduced to 1/30 that of the cathode with the GDC–LNF composite active layer. The R_{inf} at 800 °C for the cathode with the Pr_6O_{11}–LNF composite active layer was reduced to 1/8 that of the cathode with the GDC–LNF composite active layer. The R_{inf} values of the cathode with an active layer between 650 and 750 °C were also much better than those of the cathode with the GDC–LNF composite active layer. By using the cathode with the Pr_6O_{11} active layer, the operating temperature can be reduced to 700 °C while retaining the same performance (same overvoltage at 254 mA/cm^2) as a cathode with a GDC–LNF composite active layer at 800 °C.

We also investigated the reactions at the interfaces in the sintering process. X-ray diffraction (XRD) analysis revealed that the Pr_6O_{11} reacted easily with zirconia, and $Pr_2Zr_2O_7$ was produced at 1000 °C or above. It was suggested that the sintering temperature of the cathodes with the active layer could be increased to around 1000 °C without any reaction at the interface between Pr_6O_{11} and other materials.

1. Introduction

We have been investigating $LaNi_{0.6}Fe_{0.4}O_3$ (LNF) as a cathode material for solid oxide fuel cells (SOFCs) operating at intermediate temperatures [1–7], because it has certain advantages, including high electrical conductivity, a desirable thermal expansion coefficient [1], high cathode performance [2] and excellent durability as regards chromium poisoning.[3,4] We developed an LNF cathode with an active layer consisting of LNF and $Ce_{0.1}Gd_{0.1}O_{1.95}$ (GDC) for an anode supported planar cell with a practical size and operating at around 800 °C [5,6]. In contrast, the performance of an LNF cathode is insufficient for operating temperatures of 700 °C or below [6,8,9]. Such low temperature operation is needed if we are to use low cost metallic interconnectors and thus reduce manufacturing costs [9]. We have already reported that the cathode performance can be improved by using Pr-doped ceria ($Ce_{1-x}Pr_xO_{2-\delta}$ ($x = 0.1$–0.3)) in the composite active layer [7,8]. It was shown that $Ce_{1-x}Pr_xO_{2-\delta}$ ($x = 0.1$–1.0) is a mixed conductor and its conductivity increases with increases in the Pr concentration [10,11]. The mixed conduction of the Pr-doped ceria in the active layer is thought to be a reason for improved cathode performance [10-16]. The active area for the cathode electrochemical reaction of the following formula is limited to the three-phase boundary (TPB).

* Corresponding author. Tel.: +81 46 240 4229; fax: +81 46 270 2702.
E-mail addresses: hiro.tag.0302@gmail.com, taguchi.hiroaki@lab.ntt.co.jp (H. Taguchi).

0378-7753/$ – see front matter © 2013 Published by Elsevier B.V.
http://dx.doi.org/10.1016/j.jpowsour.2013.04.141

The oxygen gas, oxide ion and electron are simultaneously available at the TPB. [9]

$$O_2 + 4e^- = 2O^{2-}$$

TPBs are usually located at the interface of a cathode particle, an electrolyte and a gas phase. With a mixed conductor on the electrolyte, the TPB expands to the entire particle surface of the mixed conductor [9,10,12–16]. This can lead to improved cathode performance. The conductivity of $Ce_{1-x}Pr_xO_{2-\delta}$ increases with Pr concentration [10,11]. Therefore, Pr_6O_{11} ($Pr_xCe_{1-x}O_{2-\delta}$ ($x = 1.0$)) is thought to be the most promising composition for the active layer in this system.

In this paper, we focus on this composition (Pr_6O_{11}) for the active layer and investigate the cathode performance using the AC impedance and current interruption methods in the 650–800 °C temperature range. In addition to the cathode with the Pr_6O_{11} active layer, we also investigated a cathode with a $Pr_xCe_{1-x}O_{2-\delta}$ ($x = 0.1, 0.3, 1.0$)–LNF composite active layer and a cathode with a GDC–LNF composite active layer for comparison. We expected the composite cathode to mitigate the thermal expansion mismatch (between the active layer and the zirconia electrolyte) [1,9,11] and the inter-diffusion (between the active layer and the zirconia electrolyte) in the cathode sintering process.

If we are to employ this material as the active layer in a practical cell, we must optimize the sintering process. The sintering temperature is one of the most important conditions [9]. In terms of mechanical strength, a higher sintering temperature is preferable [5,6,9]. But any increase in the sintering temperature may cause undesirable reactions at the interface of the materials constituting the cathode [9,17–20]. We use XRD analysis to investigate the interface reaction of Pr_6O_{11} and materials adjacent to it in the sintering process.

2. Experimental

2.1. Cathode performance test

We fabricated single cells with cathodes consisting of a 40 μm thick LNF current collection layer and a 3 μm thick active layer on a 1.0 mm thick $0.89ZrO_2$–$0.10Sc_2O_3$–$0.01Al_2O_3$ or scandia alumina stabilized zirconia (SASZ) electrolyte sheet. First, the GDC buffer layer was screen printed on the SASZ electrolyte and sintered at 1150 °C in air. Next, the active layer was screen printed and dried at 100 °C, and then an LNF current collection layer was screen printed on it and sintered at 1000 °C. The mean diameters of the LNF powder, GDC powder, and $Ce_{1-x}Pr_xO_{2-\delta}$ ($x = 0.1, 0.3, 1.0$) powder were approximately 1.3, 0.1, and 0.3 μm respectively. $Ce_{1-x}Pr_xO_{2-\delta}$ ($x = 1.0$) is Pr_6O_{11}.

We printed a Pt anode on the other side of the electrolyte and a Pt reference electrode covering the entire peripheral part of the electrolyte disk. Finally, the samples were fired at 1000 °C. The effective area of the anode and cathode was 0.785 cm^2.

Fig. 1 shows backscattered electron images of cross sections of three types of cells obtained near the active layer. These cells have cathodes with a GDC–LNF composite active layer, a $Ce_{1-x}Pr_xO_{2-\delta}$ ($x = 0.1, 0.3, 1.0$)–LNF composite active layer, and a Pr_6O_{11} active layer. Fig. 1(a) shows a cathode whose active layer is a GDC (50wt%) and LNF (50 wt%) composite [5]. It has a similar layer structure to our conventional cell, but has a GDC buffer layer. Fig. 1(b) shows a cathode whose active layer is a composite of $Ce_{1-x}Pr_xO_{2-\delta}$ ($x = 0.1, 0.3, 1.0$) (50 wt%) and LNF (50 wt%). The cathode shown in Fig. 1(c) has a Pr_6O_{11} ($Ce_{1-x}Pr_xO_{2-\delta}$ ($x = 1.0$)) active layer (without LNF particles in the active layer). A GDC buffer layer was used to prevent any reaction between the SASZ electrolyte and LNF or Pr_6O_{11}. We obtained Pr_6O_{11} powder from Kojundo Chemical Lab. Co. Ltd., $0.92ZrO_2$-$0.08Y_2O_3$ (8YSZ) powder from Tosoh Corp., LNF powder from POWLEX Co., Ltd., GDC powder from ANAN KASEI Co. Ltd., and $Ce_{1-x}Pr_xO_{2-\delta}$ ($x = 0.1, 0.3$) powder from Seimi Chemical Co. Ltd.

Each electrolyte supported single cell was placed in a tester and heated to 800 °C. Humidified H_2 was supplied to the anode, and O_2 was supplied to both the cathode and reference electrode. We used glass to seal the H_2 and O_2 in the tester. The interface resistance was measured using the three-terminal AC impedance method under an open-circuit voltage. Constant current loading of 200 mA (254 mA/cm^2) for the durability test and high current loading (between 0 and 1200 mA) or 1500 mA (1529–1911 mA/cm^2) for the overvoltage tests were applied to the cells then it was terminated. We performed AC impedance measurements 60 min after termination. A Solartron SI-1260 impedance analyzer was used. The AC current frequency was swept from 10^5 to 10^{-1} Hz. The symmetrical geometry of the reference electrode, cathode, and anode enabled us to minimize any AC impedance measurement error [5,8] caused by the misalignment of the cathode and anode [5,8], which was estimated to be 0.1 mm. The overvoltage of the cathodes was measured by the current interruption method. First the current loading was raised to the maximum value, the current was then fixed for 120 min, and finally cut with a mercury contact relay. The transient waveform of the voltage between the cathode and the reference electrode after the current interruption was recorded using a digital oscilloscope. The cathode overvoltage was estimated by subtracting the ohmic drop from the cathode voltage change at the current interruption. Then the current loading was reduced to the next value. After maintaining this current value for 30 min, we performed the next interruption measurement. These sequences were repeated until the DC current was reduced to zero (the open-circuit voltage (OCV) condition).

2.2. Interface stability in sintering process

The samples used for studying the interface reaction were prepared as follows.

The starting materials including Pr_6O_{11}, LNF, GDC and 8YSZ were ball milled with zirconia balls and ethanol for 24 h and dried. Then the Pr_6O_{11} powder was mixed with LNF, GDC or 8YSZ powder (50 wt% each) in an agate motor. The mixed powers were sintered in air for 2 h at various temperatures between 900 and 1300 °C. Then the samples were ground in the agate motor. The phase and crystal structure of the samples was analyzed by XRD (Rigaku Rint 2000). The mass fraction of the phases of the sintered samples was estimated by the Rietveld method (using RIQAS software produced by Material Data Inc.). Crystal structure information contained in the Inorganic Crystal Structure Database (ICSD) database was used for the Rietveld analysis. The X-ray conditions were 30 kV and 50 mA. We used the FT scanning mode, and the range and speed of 2θ were 10–90° and 1.0° degree per minute (0.02° per step), respectively.

3. Results and discussion

3.1. Interface resistance of three types of cathodes

Fig. 2 shows impedance plots obtained at 800 °C for cathodes with a Pr_6O_{11} active layer ($Pr_xCe_{1-x}O_{2-\delta}$ ($x = 1.0$)), a $Pr_xCe_{1-x}O_{2-\delta}$ ($x = 0.1, 0.3, 1.0$) and LNF composite active layer, and a GDC and LNF composite active layer. We evaluated the cathode interface resistance, R_{inf}, from the diameter of each impedance plot semicircle. R_{inf} for the cathode with the Pr_6O_{11}–LNF composite active layer was 1/8 that of the cathode with the GDC–LNF composite active layer. This cathode exhibited the smallest R_{inf} of all the

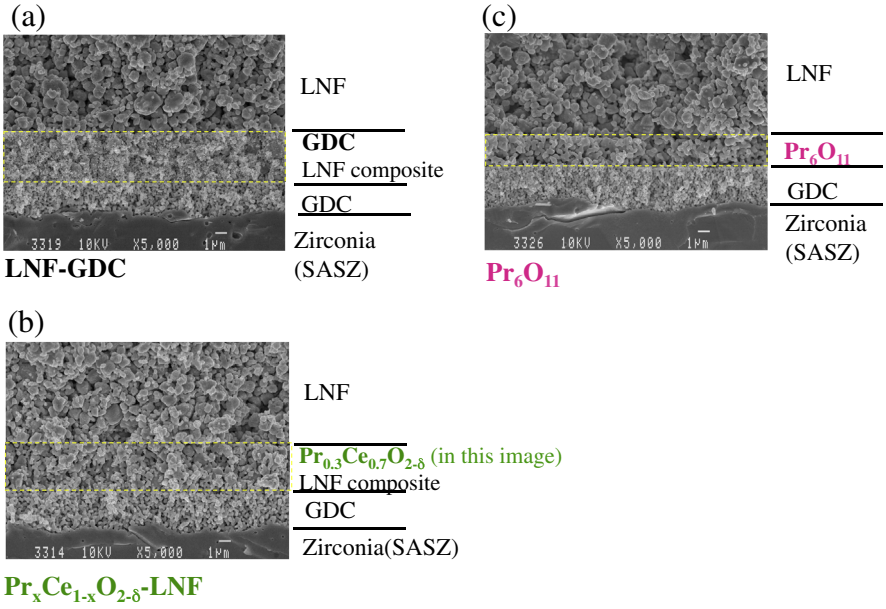

Fig. 1. Cross-section of three types of cathode near the electrolyte. (a) Cathode with GDC–LNF composite active layer, (b) cathode with $Pr_xCe_{1-x}O_{2-\delta}$ (x = 0.1, 0.3, 1.0)–LNF composite active layer, and (c) cathode with Pr_6O_{11} active layer.

cathodes with a $Pr_xCe_{1-x}O_{2-\delta}$ (x = 0.1, 0.3, 1.0)–LNF composite active layer. This appears to be caused by the higher mixed conduction in $Ce_{1-x}Pr_xO_{2-\delta}$ with a larger x [8,10,11]. It is considered that the mixed conduction in the $Ce_{1-x}Pr_xO_{2-\delta}$ expanded the TPB in the cathode and resulted in the high cathode performance [10–16]. The ohmic resistance (left hand side value of the semicircle) also decreased slightly with x. We currently have no good explanation for this. It might be explained as follows; the expansion of the TPB mitigated the current constriction near the TPB (especially on the GDC buffer layer side), which contributed to the reduction in ohmic resistance.

The R_{inf} for the cathode with the Pr_6O_{11} active layer was 1/30 that of the cathode with the GDC–LNF composite active layer. This shows that the cathode with an active layer consisting of only this mixed conductor is the best in terms of the R_{inf}. The mixed conducting particles (in this case, Pr_6O_{11} particles) directly connected to the GDC buffer layer are thought to contribute to the cathode reaction [9]. The cathode with the Pr_6O_{11} active layer has the largest number of mixed conducting particles near the electrolyte among the three types of cathodes. These results demonstrated that using Pr_6O_{11} in the active layer is very effective for improving the cathode interface resistance.

After this, we focused on the cathode with the Pr_6O_{11} active layer and the cathode with the Pr_6O_{11} and LNF composite active layer. Fig. 3(a)–(c) shows the AC impedance plots for those cathodes at 750 and 650 °C. The results for the LNF cathode with the GDC–LNF composite active layer are also shown for comparison. The cathode with the Pr_6O_{11} active layer and the cathode with the Pr_6O_{11}–LNF composite active layer have much smaller R_{inf} values than those of the cathode with the GDC–LNF composite active layer in this temperature rage. The R_{inf} values of those cathodes are plotted against temperature in Fig. 4. The $\log_e(R_{inf})$ values for all the cathodes have an almost linear relation with temperature. The temperature dependence of R_{inf} is almost the same for all the cells. Using cathodes with an active layer containing Pr_6O_{11} enables us to reduce the operating temperature from 800 °C to 720 °C or 680 °C without increasing R_{inf}.

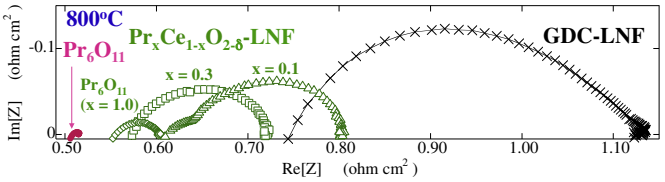

Fig. 2. AC impedance plots for cathodes with different active layers. The effective area was 0.785 cm^2.

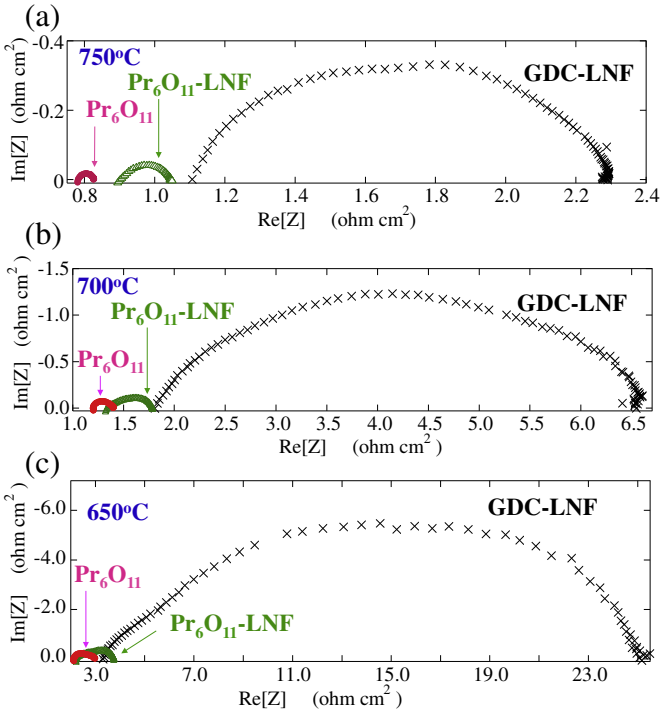

Fig. 3. (a) AC impedance plots for three types of cathode at 750 °C. (b) AC impedance plots for three types of cathode at 700 °C. (c) AC impedance plots for three types of cathode at 650 °C.

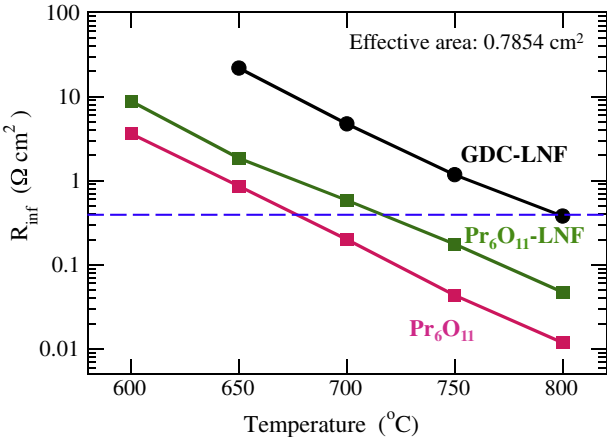

Fig. 4. Temperature vs. interface resistance, R_{inf}.

R_{inf} is a very important index for cathode performance, particularly at a low current density. However, R_{inf} is constant only near the OCV potential. The performance under practical conditions is usually different. Therefore, the cathode performance at a practical current density was investigated with the current interruption method.

In Fig. 5(a)–(c), the overvoltages evaluated by the current interruption method are plotted against the current density. The overvoltages of the cathode with the Pr_6O_{11} active layer and the cathode with the Pr_6O_{11}–LNF composite active layer are much smaller than that of the cathode with the GDC–LNF composite active layer at all current densities. The performance of the cathode with the Pr_6O_{11} active layer is better than that of the cathode with the Pr_6O_{11}–LNF composite active layer. This order of performance of the three types of cathodes at each temperature is the same between 700 and 800 °C. And these results are consistent with the results for R_{inf} shown in Fig. 3.

This shows that cathodes with an active layer containing Pr_6O_{11} perform much better than an LNF cathode with a GDC–LNF composite active layer at a practical current density.

3.2. Overvoltage of three types of cathodes

The overvoltage values at 254 mA/cm^2 are plotted against the operating temperature in Fig. 6. The overvoltage of the cathodes with the Pr_6O_{11} active layer at 700 °C is lower than that for the cathode with the GDC–LNF active layer at 800 °C. By using the cathode with the Pr_6O_{11} active layer, the operating temperature can be reduced to 700 °C while maintaining the same cathode performance. This means that introducing a Pr_6O_{11} active layer enables us to reduce the operating temperature by 100 °C. The advantage of a cathode with Pr oxide tends to be smaller at lower temperatures. The result is slightly different from the interface resistance results. This may be because the overvoltage and current density have a nonlinear relationship at a high current density. Therefore, the difference in the cathode performance tends to be significant under very low current density and OCV conditions. The steeper slope of the cathode with the Pr_6O_{11} active layer compared with the other cathodes may originate from the fact that the temperature dependence of the conductivity in Pr_6O_{11} is more sensitive than in a composite active layer or an LNF layer [11].

Fig. 7 shows the temporal change of the cathode potential against the reference electrode at 800 °C. This cathode has a Pr_6O_{11} active layer. The initial point ($t = 0$) represents the starting point of the current loading of 254 mA/cm^2. The cathode potential was stable from the beginning of the test. This shows that there is no initial current

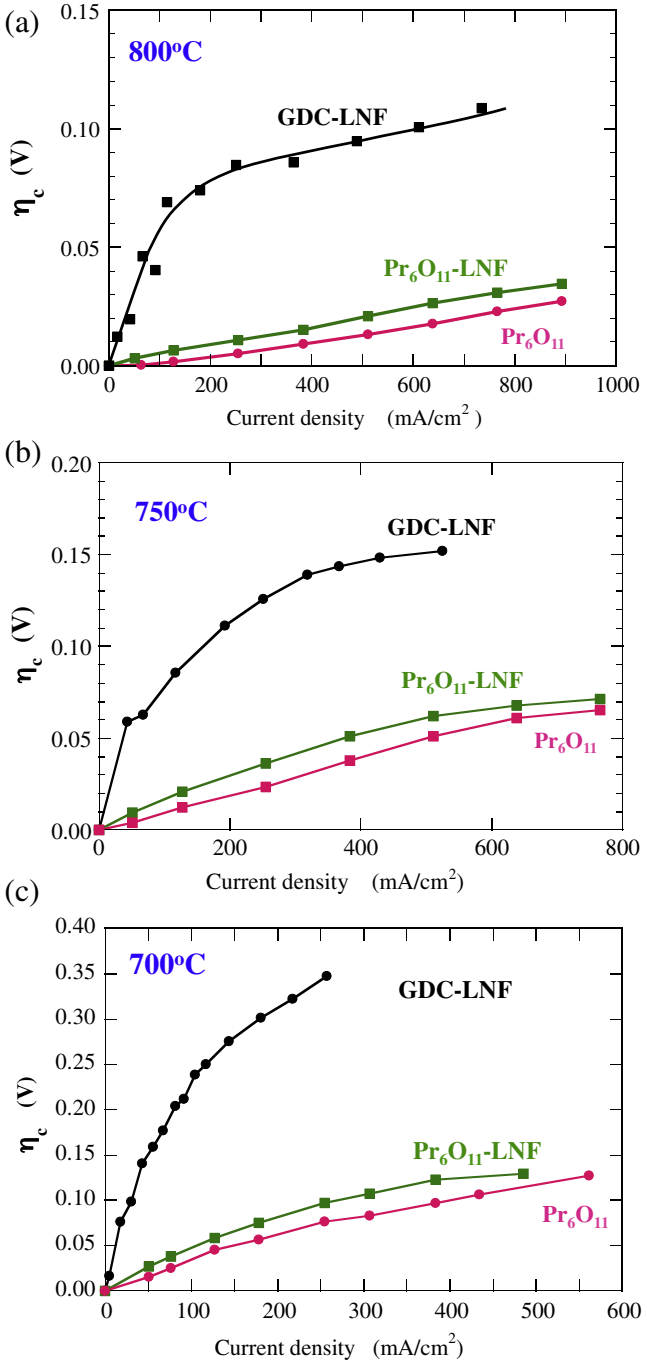

Fig. 5. (a) Overvoltage for three types of cathode at 800 °C. (b) Overvoltage for three types of cathode at 750 °C. (c) Overvoltage for three types of cathode at 700 °C.

loading effect associated with $La_2Zr_2O_7$. [21] After 65–85 h the potential changed greatly in the high current density test. Even after the high current density test, the cathode potential retained its value. This shows that this cathode configuration is durable under practical current loading conditions. After this test, the operating temperature was reduced to 750 °C or lower to conduct interface resistance and overvoltage measurements at lower temperatures.

3.3. Reaction of interface between Pr_6O_{11} and materials in cathode

Pr_6O_{11} and $Ce_{1-x}Pr_xO_{2-\delta}$ particles are incorporated in the active layer. These particles might react with the LNF or GDC. If the GDC

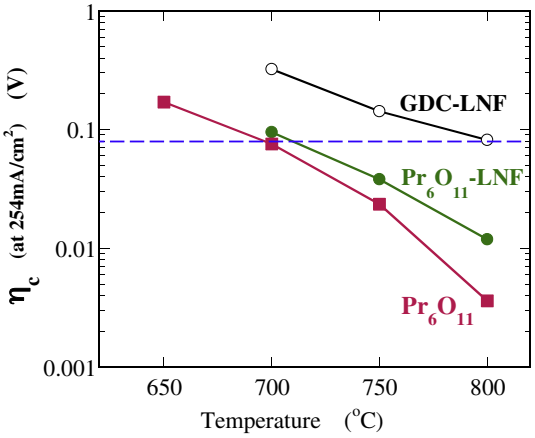

Fig. 6. Temperature vs. overvoltage at 254 mA/cm^2.

buffer layer does not function adequately, Pr_6O_{11} and $Ce_{1-x}Pr_xO_{2-\delta}$ might react with the SASZ zirconia electrolyte. We examined the sintering temperature dependence of the reactivity between Pr_6O_{11} and LNF, GDC, and 8YSZ.

3.3.1. Reaction of interface between Pr_6O_{11} and 8YSZ

The GDC buffer layer is porous because of its poor sinterability. In addition, the GDC buffer layer should be as thin as possible to reduce ohmic loss. Because of this, we need to consider the reaction between Pr_6O_{11} or $Ce_{1-x}Pr_xO_{2-\delta}$ and SASZ zirconia electrolyte. Pr_6O_{11} and 8YSZ powders were selected for this reaction, because of the availability of 8YSZ powder. We used 8YSZ rather than SASZ because it is much more widely used than SASZ. 8YSZ and SASZ have basically the same crystal structure and the main elements (Zr and O) are the same. The only difference is the additive (Sc or Y). Zr, La Pr and Ce atoms are involved in the reaction between zirconia electrolyte and other material. Therefore, we think that the effect of using different additive elements is negligible. The XRD patterns for mixtures of Pr_6O_{11} and 8YSZ (50 wt% and 50 wt%) sintered at various temperatures are shown in Fig. 8. The peaks in the XRD pattern at 900 °C were assigned to the cubic phase of YSZ (S.G. F m-3 m (No. 225), ICSD# 173694) and the monoclinic phase of Pr_6O_{11} (S.G. P 1 21/c 1 (No. 14), ICSD# 82107). They are peaks for the starting materials. The pattern changed at 1000 °C and became obvious at 1100 °C or above. The peaks at 1300 °C were assigned to the reaction product of $Pr_2Zr_2O_7$ (S.G. F d-3 m Z (No. 227), ICSD# 150207). Figs. 9 and 10 show the mass fraction and unit cell volume of the identified phases, respectively. They were estimated by the Rietveld method. The mass fraction of $Pr_2Zr_2O_7$ started increasing at 1000 °C and increased

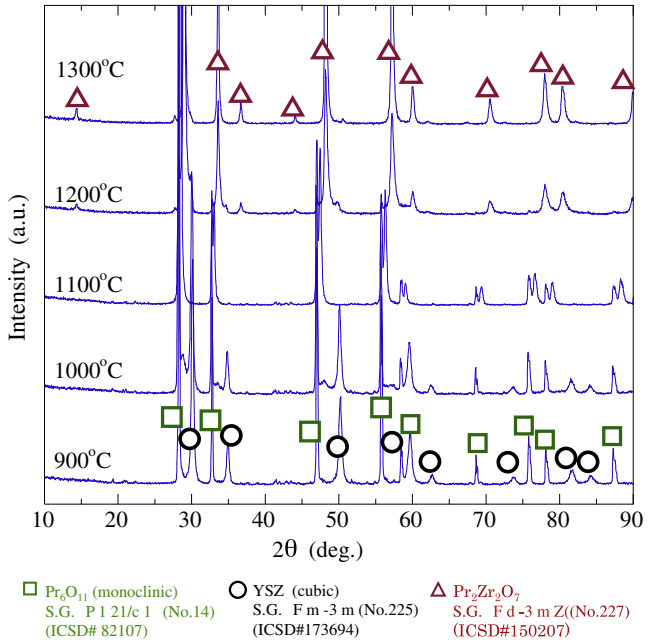

Fig. 8. XRD patterns for mixture of Pr_6O_{11} and 8YSZ sintered at difference temperatures. Square, circles and triangles indicate Pr_6O_{11}, YSZ and $Pr_2Zr_2O_7$ phases, respectively.

monotonically with the sintering temperature as shown in Fig. 9. $Pr_2Zr_2O_7$ is a *pyrochlore, which is a typical reaction product of perovskite cathode material and zirconia. This material sometimes causes the cathode properties to degrade. When an active layer containing Pr_6O_{11} is used without the GDC buffer layer $Pr_2Zr_2O_7$ forms* and this results in degradation of the cathode [8,9]. The unit cell volumes for Pr_6O_{11} and 8YSZ are plotted against the sintering temperature in Fig. 10. The unit cell volume change represents the lattice constant change. When the sintering temperature exceeded 900 °C, the behavior of the unit cell volumes of Pr_6O_{11} and 8YSZ reversed, namely the cell volume of Pr_6O_{11} decreased, and that of 8YSZ increased. This shows that there is inter-diffusion of the Pr and Zr atoms at the interface between Pr_6O_{11} and 8YSZ, because the ionic radius of Pr^{4+} is larger than that of Zr^{4+}. Specifically, the ionic radii for Pr^{4+}(coordination number: 8) and Zr^{4+} (coordination number: 8) are 0.96 and 0.84 Å, respectively [22].

3.3.2. Reaction of interface between Pr_6O_{11} and GDC

XRD patterns of the samples used for the reaction of Pr_6O_{11} and GDC are shown in Fig. 11. The peaks for 900 °C were assigned to the

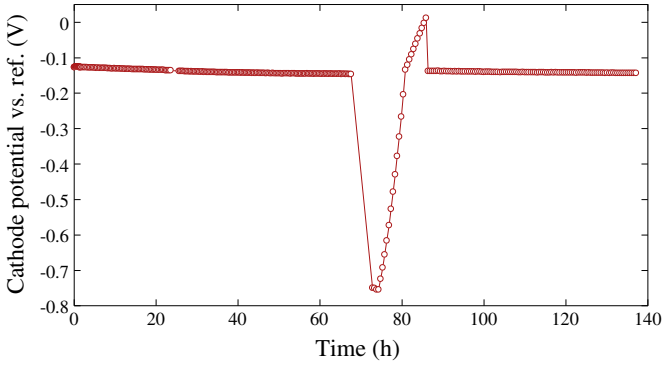

Fig. 7. Temporal change of the cathode potential of a cathode with a Pr_6O_{11} active layer operated at 254 mA/cm^2 at 800 °C.

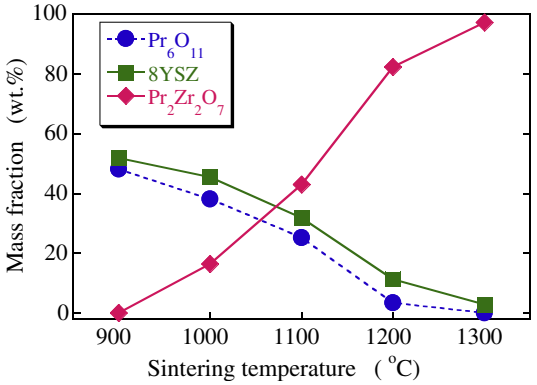

Fig. 9. Sintering temperature vs. mass fraction of the identified phases (Pr_6O_{11}, 8YSZ, and $Pr_2Zr_2O_7$.) after sintering the mixture of LNF and Pr_6O_{11}.

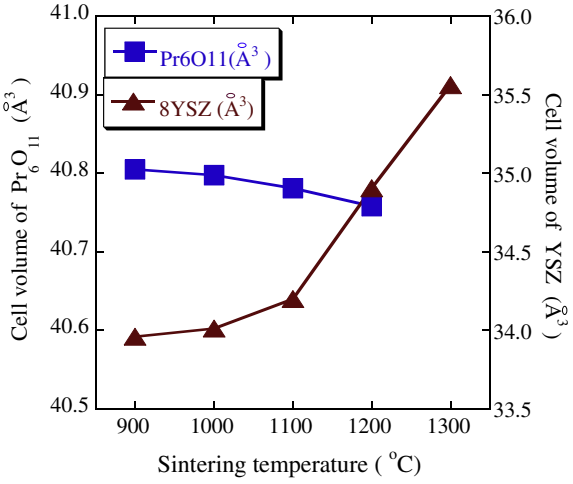

Fig. 10. Sintering temperature vs. cell volume of Pr_6O_{11} and 8YSZ phases.

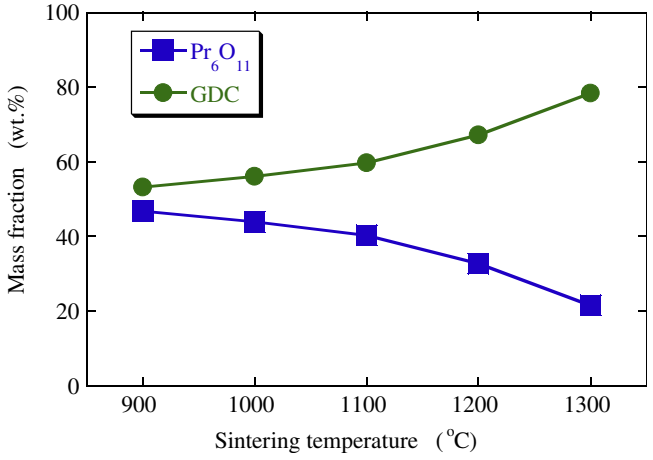

Fig. 12. Sintering temperature vs. mass fraction of the identified phases (Pr_6O_{11}, GDC of Ce(Gd, Pr)$O_{2-\delta}$.) after sintering the GDC and Pr_6O_{11} mixture.

starting materials of the cubic phase of GDC (S.G. F m-3 m (No. 225), ICSD# 28795) and the monoclinic phase of Pr_6O_{11}. They are in the fluorite structure and have similar XRD patterns. The higher angles of the perturbs are shown. They form a solid solution of Ce(Gd,Pr)$O_{2-\delta}$. Fig. 11 shows that the solid solution reaction proceeded as the sintering temperature increased. The mass fraction of the phases are plotted in Fig. 12. The mass fraction change is significant at 1100 °C and above. The GDC and solid solution of Ce(Gd,Pr)$O_{2-\delta}$ are in the cubic phase, whereas Pr_6O_{11} is in the monoclinic phase. Therefore, the fractions of the GDC and Ce(Gd,Pr)$O_{2-\delta}$ phases cannot be distinguished. The GDC or Ce(Gd,Pr)$O_{2-\delta}$ fraction increased at high sintering temperatures. And the fraction of the Pr_6O_{11} phase decreased under high temperature sintering conditions. The unit cell volumes of these phases are plotted in Fig. 13. The unit cell volumes of both phases decreased. This is because the solid solution of Ce(Gd,Pr)$O_{2-\delta}$ has a smaller unit cell volume than the end members (GDC and Pr_6O_{11}). The inter-diffusion of the Pr and Ce atoms at the interface becomes faster above 1100 °C. This is consistent with the result in Fig. 12. Regarding the interface of GDC and Pr_6O_{11} the sintering temperature should be as low as possible to prevent the reaction from occurring. Because the solid solution is also an active material as an SOFC cathode, increasing the temperature would not cause any serious problems. However, the interface resistance and overvoltage of those cathodes would be larger than those sintered at lower temperatures.

3.3.3. *Reaction of interface between Pr_6O_{11} and LNF*

The XRD patterns of the samples used for the reaction of Pr_6O_{11} and LNF are shown in Fig. 14. The peaks for 900 °C were assigned to the starting materials of the rhombohedral phase of LNF (S.G. R-3 c H (No. 167), ICSD# 84937) and the monoclinic phase of Pr_6O_{11}. In addition to the phases of the starting materials, the orthorhombic phases of $La_4(Ni,Fe)_3O_{10}$ (S.G. F m m m (No. 69), ICSD# 80279) and $La_2(Ni,Fe)O_{4.18}$ (S.G. B b c m (No. 64), ICSD# 44252) were identified in a sample sintered at 1300 °C. The mass fractions of the phases for the sintered samples are plotted in Fig. 15. The mass fraction change was not significant at 1000 °C. Even at 1100 °C, the change was very slight.

The reaction products of $La_4(Ni,Fe)_3O_{10}$ and $La_2(Ni,Fe)O_{4.18}$ increased at 1200 °C. This showed that the reaction between LNF and Pr_6O_{11} proceeded at 1200 °C. But this reaction appears to proceed slowly at this temperature. The unit cell volumes of the starting materials are plotted in Fig. 16. The unit cell volumes of

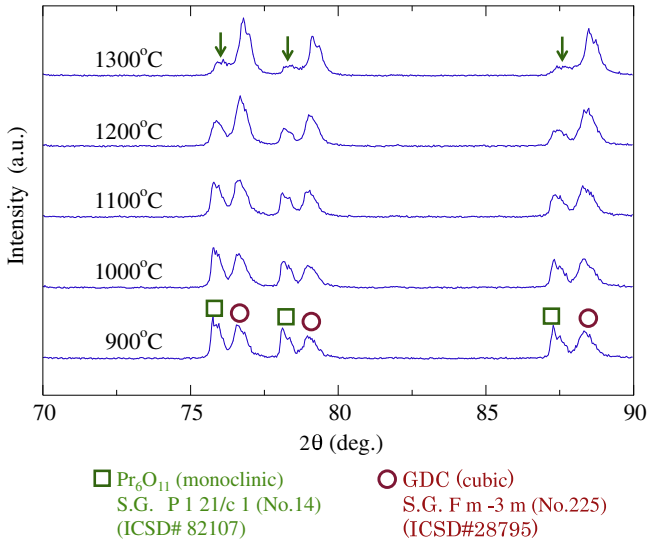

Fig. 11. XRD patterns for mixture of Pr_6O_{11} and GDC sintered at different temperatures. Squares and circles indicate Pr_6O_{11} and GDC phases, respectively.

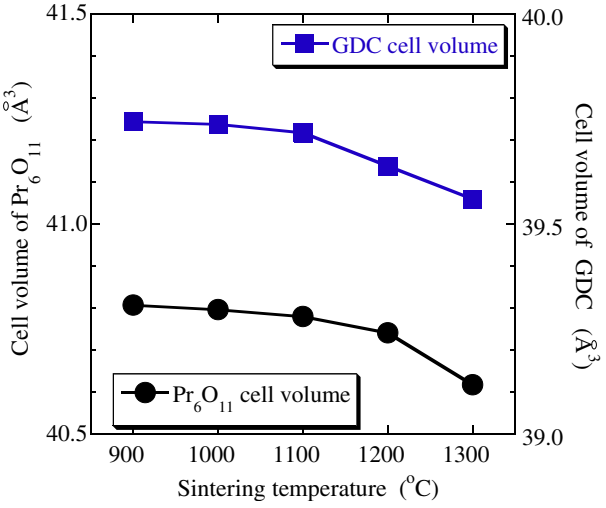

Fig. 13. Sintering temperature vs. cell volume of Pr_6O_{11} and GDC phases.

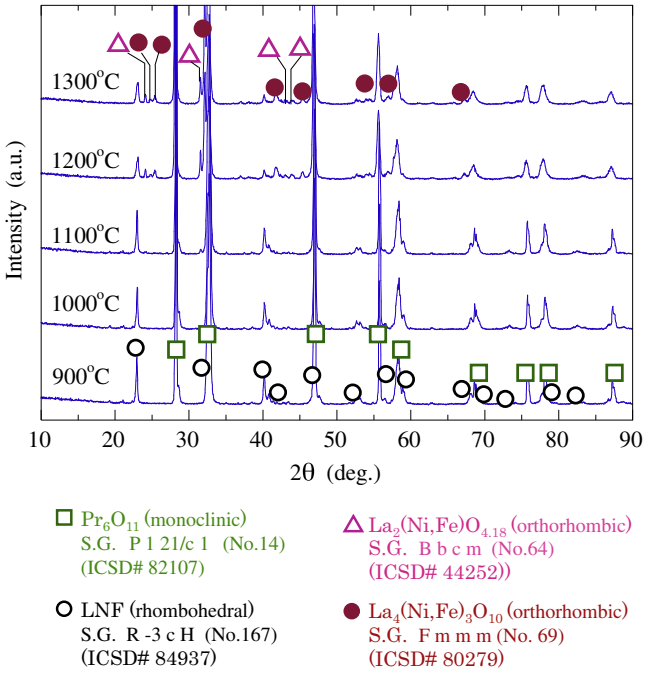

Fig. 14. XRD patterns for mixture of Pr_6O_{11} and LNF fired at difference temperatures. Open squares, open circles open triangles and filled circles indicate Pr_6O_{11}, LNF, $La_2(Ni,Fe)O_{4.18}$ phases, respectively.

both phases were almost constant up to 1100 °C and increased from 1200 °C. Above 1200 °C, the unit cell volumes of both LNF and Pr_6O_{11} were constant. This temperature dependence is close to that shown in Fig. 15. The mechanism of this reaction is illustrated in Fig. 17. The $La_2(Ni,Fe)O_{4.18}$ phase was initially created at 1100 °C, but this phase did not increase greatly with sintering temperature. The $La_4(Ni,Fe)_3O_{10}$ phase increased greatly from 1200 °C. The Pr atoms initially diffused into the LNF and created an A-site excess. $(La(Pr))_2(Ni,Fe)O_{4.18}$ was created at the interface. The final product of $(La(Pr))_4(Ni,Fe)_3O_{10}$ at high temperature was created by diffusing the Pr atoms from $(La(Pr))_2(Ni,Fe)O_{4.18}$. As regards the LNF and Pr_6O_{11} interface, to avoid the reaction, the sintering temperature should not be increased to 1200 °C. On the Pr_6O_{11} side, the diffusion of La^{3+} into Pr_6O_{11} may cause an oxygen vacancy increase. But the ionic conductivity of La doped Pr_6O_{11} may not be high, because of the large difference between the ionic radii of La^{3+} and Pr^{4+}.

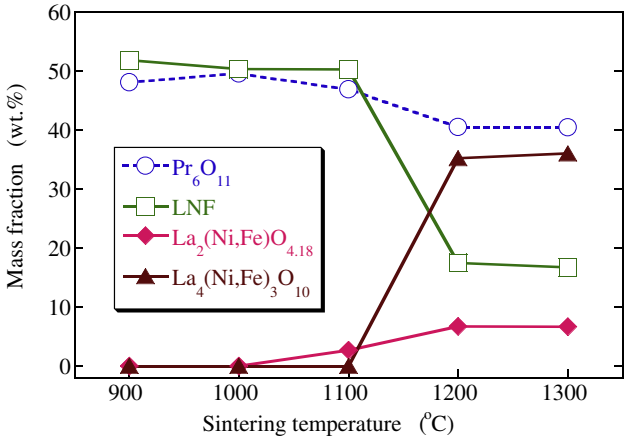

Fig. 15. Mass fraction of the identified phases after sintering the LNF and Pr_6O_{11} mixture.

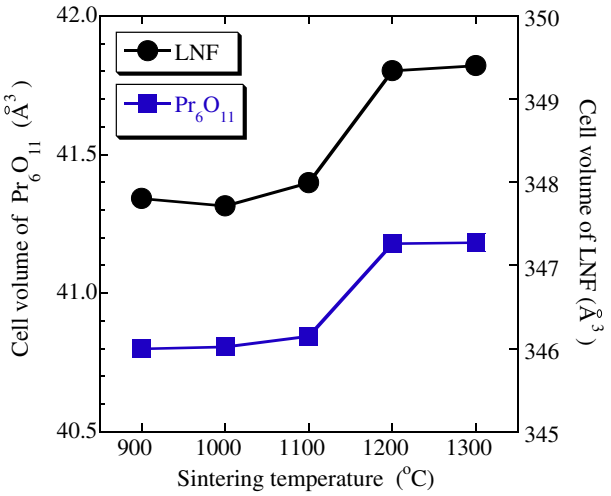

Fig. 16. Sintering temperature dependence of the unit cell volume of the Pr_6O_{11} and LNF phases.

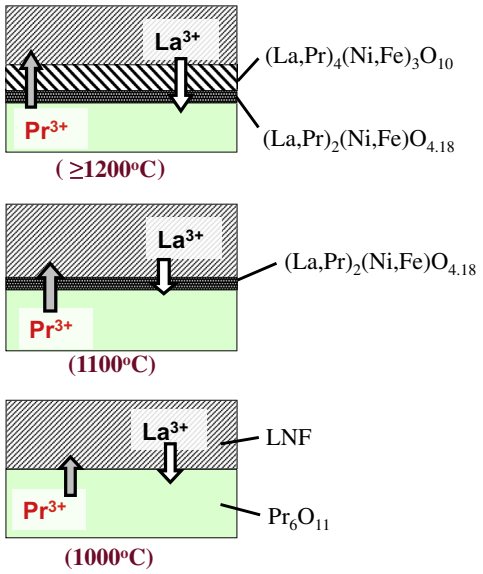

Fig. 17. Schematics of the reaction of Pr_6O_{11} and LNF at 1000, 1100 and 1200 °C or above.

4. Conclusions

We fabricated electrolyte supported single cells with three types of cathodes. They were a cathode with a Pr_6O_{11} ($Pr_xCe_{1-x}O_{2-\delta}$ ($x = 1.0$)) active layer, a cathode with a $Pr_xCe_{1-x}O_{2-\delta}$ ($x = 0.1$, 0.3, 1.0)–LNF composite active layer (composite of $Pr_xCe_{1-x}O_{2-\delta}$ ($x = 0.1$, 0.3, 1.0) and LNF), and a cathode with a GDC–LNF composite active layer. Their electrochemical properties as an SOFC cathode were investigated by the AC impedance method and the current interruption method. The reactions that occurred during the cathode sintering process between Pr_6O_{11} and other materials in the cathode were also investigated. We used X-ray powder diffraction analysis to study interface reactions.

1. The R_{inf} of cathodes with a $Pr_xCe_{1-x}O_{2-\delta}$ ($x = 0.1$, 0.3, 1.0)–LNF composite active layer decreased with increases in x. At 800 °C, the R_{inf} value of a cathode with an active layer consisting of PDC–LNF composite (composite of $PrO_{2-\delta}$ and LNF) was 1/8

that of a cathode with GDC–LNF composite active layer. At 800 °C, the R_{inf} of a cathode with a Pr_6O_{11} active layer was reduced to 1/30 that of a cathode with a GDC–LNF composite active layer.

2. The overvoltage at 254 mA/cm^2 and 800 °C of cathodes with a Pr_6O_{11}–LNF composite active layer and a cathode with a Pr_6O_{11} active layer were 1/6.9 (11.9 mV) and 1/22 (3.6 mV), respectively, of that of a cathode with a GDC–LNF composition active layer (81.6 mV). By using a cathode with a Pr_6O_{11} active layer, the operating temperature can be reduced to 700 °C while realizing the same performance as a cathode with a GDC–LNF composite active layer at 800 °C.
3. The reaction of Pr_6O_{11} and 8YSZ was significant from 1000 °C. This result showed that we need a GDC buffer layer between the active layer and the electrolyte. The reaction between LNF and Pr_6O_{11} was not significant up to 1100 °C. At higher sintering temperatures A-site excess perovskite products such as $(La(Pr))_2(Ni,Fe)O_{4.18}$ and $(La(Pr))_4(Ni,Fe)_3O_{10}$ were created at the interface between LNF and Pr_6O_{11}. The reaction between Pr_6O_{11} and GDC proceeded from 900 °C and a solid solution of $Ce_{1-x}Pr_xO_{2-\delta}$ was created. Cathodes with an active layer containing Pr_6O_{11} should be sintered at 1100 °C or below. A sintering temperature of 1000 °C or below is preferable, with respect to the interface reaction.

Acknowledgments

We thank Yoshio Ohki for his help with the sample preparation and cathode property measurements.

References

[1] R. Chiba, F. Yoshimura, Y. Sakurai, Solid State Ionics 124 (1999) 281–288.
[2] H. Orui, K. Watanabe, R. Chiba, M. Arakawa, Journal of Electrochemical Society 151 (9) (2004) A1412–A1417.
[3] T. Komatsu, H. Arai, R. Chiba, K. Nozawa, M. Arakawa, K. Sato, Electrochemical and Solid-State Letters 9 (1) (2006) A9–A12.
[4] T. Komatsu, H. Arai, R. Chiba, K. Nozawa, M. Arakawa, K. Sato, Journal of Electrochemical Society 154 (4) (2007) B379–B382.
[5] R. Chiba, Y. Tabata, T. Komatsu, H. Orui, K. Nozawa, M. Arakawa, K. Sato, H. Arai, Journal of Electrochemical Society 155 (6) (2008) 575–580.
[6] H. Orui, K. Nozawa, K. Watanabe, S. Sugita, R. Chiba, T. Komatsu, H. Arai, M. Arakawa, Journal of Electrochemical Society 155 (2008) B1110–B1116.
[7] R. Chiba, T. Komatsu, H. Orui, H. Taguchi, K. Nozawa, H. Arai, Journal of Korean Ceramic Society 45 (12) (2008) 766–771.
[8] R. Chiba, T. Komatsu, H. Orui, H. Taguchi, K. Nozawa, H. Arai, Electrochemical and Solid-State Letters 12 (5) (2009) B69–B72.
[9] N.Q. Minh, Journal of American Ceramic Society 76 (1993) 563.
[10] S. Lübke, H.-D. Wiemhöfer, Solid State Ionics 117 (1999) 229.
[11] R. Chiba, H. Taguchi, T. Komatsu, H. Orui, K. Nozawa, H. Arai, Solid State Ionics 197 (2011) 42–48.
[12] A. Esquirol, N.P. Brandon, J.A. Kilner, M. Mogensen, Journal of Electrochemical Society 151 (11) (2004) A1847–A1855.
[13] M.J. Jørgensenz, M. Mogensen, Journal of Electrochemical Society 148 (2001) A433.
[14] M. Kyoyama, C. Wen, T. Masuyama, J. Otomo, H. Fukunaga, K. Yamada, K. Eguchi, H. Takahashi, Journal of Electrochemical Society 148 (2001) A795.
[15] T. Kawada, J. Suzuki, M. Sase, A. Kaimai, K. Yashiro, Y. Nigara, J. Mizusaki, K. Kawamura, H. Yugami, Journal of Electrochemical Society 149 (2002) E252.
[16] T. Nakamura, K. Yashiro, A. Kaimai, T. Otake, K. Sato, T. Kawada, J. Mizusaki, Journal of Electrochemical Society 155 (2008) B1244.
[17] A. Weber, R. Manner, E. Ivers-Tiffee, Denki Kagaku 64 (1996) 582.
[18] E. Ivers-Tiffee, A. Weber, K. Schmid, V. Krebs, Solid State Ionics 174 (2004) 223.
[19] A. Mai, V.A.C. Haanapple, S. Uhlenbruck, F. Tietz, D. Stover, Solid State Ionics 176 (2005) 1341.
[20] Y. Matsuzaki, I. Yasuda, Solid State Ionics 152–153 (2002) 463.
[21] R. Chiba, Y. Tabata, T. Komatsu, H. Orui, K. Nozawa, M. Arakawa, H. Arai, Solid State Ionics 178 (2008) 1701–1709.
[22] R.D. Shannon, Acta Crystallography Section A 32 (1976) 751.